Interface Structural Defects and Photoluminescence Properties of Epitaxial GaN and AlGaN/GaN Layers Grown on Sapphire

V. P. Klad'ko[a], S. V. Chornen'kii[a], A. V. Naumov[a]^, A. V. Komarov[b],
M. Tacano[c], Yu. N. Sveshnikov[d], S. A. Vitusevich[a], and A. E. Belyaev[a]

[a]*Lashkarev Institute of Semiconductor Physics, National Academy of Sciences of Ukraine, Kiev, 03028 Ukraine*
^*e-mail: naumov@ifpht.kiev.ua*
[b]*Institute of Physics, National Academy of Sciences of Ukraine, Kiev, 03028 Ukraine*
[c]*AMRC, Meisei University, Hino, Tokyo, 191-8506 Japan*
[d]*ZAO Élma–Malakhit, Zelenograd, 124460 Russia*
Submitted January 11, 2006; accepted for publication January 25, 2006

Abstract—Overall characterization of the GaN and AlGaN/GaN epitaxial layers by X-ray diffractometry and optical spectral analysis is carried out. The layers are grown by metalloorganic gas-phase epitaxy on (0001)-oriented single crystal sapphire wafers. The components of strains and the density of dislocations are determined. The effects of strains and dislocations on the photoluminescence intensity and spectra are studied. The results allow better understanding of the nature and mechanisms of the formation of defects in the epitaxial AlGaN/GaN heterostructures.

1. INTRODUCTION

The progress of the present-day semiconductor physics and technology, specifically quantum electronics and optoelectronics depends to a large extent on the technology of high-quality semiconductor materials and the development of perfect epitaxial heterostructures with specified physical properties [1, 2]. The high quality of such heterostructures (HSs) is defined primarily by the minimal elastic strains and the absence of plastic strains in the active (working) region, while the efficiency and reliability of operation of HS-based devices depend on the localization and density of active impurity defects and structural defects at the heterointerface and in the working region.

In the course of epitaxial growth, the heterolayers and films can be matched to the technological wafer coherently or incoherently. In the case of the coherent (so-called pseudomorphic) growth of the starting layer, the mismatch of the lattice parameters of the film and wafer does not give rise to misfit dislocations.

Under deviations from the conditions of coherent growth with increasing film thickness, relaxation of elastic strains in the system gives rise to misfit dislocations. In addition to the increase in the density of dislocations, nonuniformities in their distribution in the heterointerface plane appear. Plastic strain resulting from of uncompensated stresses and linear structural defects in the system is the final consequence of the incoherent growth. In this case, the semiconductor properties of the system prescribed by the initial alloy composition and, hence, by the mismatch between the lattice parameters are modified. Therefore, there is some correlation between the structural characteristics (mismatch between the lattice parameters, elastic stresses, and plastic strain) of epitaxial HSs and the physical properties and parameters such as the band gap, the half-width and peak energy of the edge luminescence band, the quantum yield of radiative recombination, the character of polarization of the emission, etc. [3].

In the last few years, HSs based on the III-Group nitrides have attracted considerable interest. Such HSs are widely used for the development of injection lasers and light-emitting diodes for the short-wavelength region of the spectrum. These HSs are thought to be promising for applications in high-voltage microelectronics and high-frequency microelectronics [4]. Specifically, GaN-based HSs (due to the wide band gap and high drift velocities) are considered as the most appropriate structures for developing field-effect transistors operating by high-mobility hot electrons (often referred to as high electron mobility transistors (HEMTs)) [5].

The GaN/AlGaN HSs are commonly grown from metal organic compounds by gas-phase epitaxy, i.e., by metal-organic chemical vapor deposition (MOCVD) on sapphire wafers in reactors with inductive heating [6]. The sources of the Ga, Al, and N elements are trimethyl gallium (TMG), trimethyl aluminum (TMA), and ammonia (NH_3); for doping, silane (SiH_4) is used, and hydrogen serves as a gas carrier. At first, a thin layer of GaN or of GaN with an admixture of Al is deposited on

the wafer at the temperature ~500°C. Then, after annealing of the initial layer at the temperatures in the range 1000–1100°C, the successive epitaxial growth of the GaN and $Al_xGa_{1-x}N$ monolayers is conducted to produce the total $Al_xGa_{1-x}N$/GaN structure (the Al content is $x = 0.1$–0.35). Under the pressure 100–200 mbar in the reactor, the deposition rate is 0.5–1.5 μm/h, depending on the molar flow of TMG and TMA. It is clear that the MOCVD procedure requires close monitoring of the growth and examination of the effects of impurities and structural defects generated in the epitaxial layers on their basic structural, electrical, and optical properties. In this context, in spite of the recent advances in the technology of nitrides, some properties of the epitaxial GaN/AlGaN HSs have not yet been adequately studied and call for comprehensive investigations by various techniques.

In this paper, we report the X-ray diffraction data on the structure of the epitaxial GaN and $Al_xGa_{1-x}N$ ($x = 0.25$) heterolayers grown by MOCVD technology on single-crystal sapphire wafers. We present also the results of the analysis of the photoluminescence (PL) spectra of these structures. The data allow us to better understand and interpret the nature and mechanisms of formation of the structure in the GaN-based epitaxial systems for HEMTs.

2. EXPERIMENTAL

The experimental samples of the GaN-based epitaxial structures were grown by the conventional procedures of low-pressure chemical vapor deposition of gas-phase metal-organic compounds on sapphire substrates. We used optically transparent (0001)-oriented single-crystal sapphire (Al_2O_3) wafers with the thickness 430 μm. Two types of samples were fabricated. The sample of the first type (sample S_1) was the AlGaN/GaN epitaxial HEMT structure that involved the basic undoped GaN layer with the thickness 2 μm and the barrier $Al_xGa_{1-x}N$ ($x = 0.25$) layer consisting of three sublayers, namely, the undoped $Al_{0.25}Ga_{0.75}N$ layer with the thickness 3 nm, the intermediate Si-doped $Al_{0.25}Ga_{0.75}N$ layer with the thickness 15 nm (the donor concentration was $N_D = 2 \times 10^{18}$ cm^{-3}), and the cladding undoped $Al_{0.25}Ga_{0.75}N$ layer with the thickness 10 nm. The experimental sample of the second type (sample S_2) was the epitaxial GaN film with the thickness 5 μm. The concentration of uncontrollable impurities in GaN was at the level of 1×10^{16} cm^{-3} [6].

The X-ray diffraction studies of the samples were carried out, as in [7], by the two- and three-axis diffractometry, with the compositional features of the structures to be studied taken into account. We varied the layout of the experiment: we recorded, correspondingly, the signals of the symmetrical Bragg diffraction (the 0002 and 0004 peaks), the symmetrical Laue diffraction (the $10\bar{1}0$ and $20\bar{2}0$ peaks), and the asymmetric diffraction (the $1\bar{1}04$ and $11\bar{2}4$ peaks). For every

peak, the diffraction curves were obtained for two directions in the section of reciprocal lattice sites, namely, in the directions orthogonal to the diffraction vector (the ω scanning) and parallel to the diffraction vector (the ω/2θ scanning).

The data were analyzed in the context of the mosaic block model [8]. According to this model, the state of strains and the defect structure of the layer are characterized by the distortion tensor components $\langle \varepsilon_{ij} \rangle$ and by the effective dimensions of the regions of coherent scattering (CS) along and across the layer, τ_x and τ_z. The relation between the coordinates in the reciprocal space (q) and the angular broadenings (w) depends on the direction of scanning with respect to the diffraction vector **H**: for scanning along the diffraction vector and along the orthogonal direction, we have $\delta\omega = \delta q_{\parallel}/k\cos\theta_B$ and $\delta\omega = \delta q_{\perp}/H$, respectively. The shape of the peaks (the peak broadening) is influenced by strains and depends on the finite dimensions of CS regions. These two effects can be separated by recognizing that the distortion components tend to broaden only the peaks that involve the corresponding diffraction vector components $\delta q_i = \langle \delta \varepsilon_{ij} \rangle H_j$, whereas the finiteness of the dimensions of CS regions influences all of the reciprocal lattice sites in a specified direction. In the Laue layout of measurements, as well as in the Bragg layout, the networks of dislocations tend to broaden the reflectance peaks in the direction normal to the diffraction vector, although the directions of the vector **H** for these two layouts differ by 90°. The finiteness of the coherence length in the directions normal to the surface ($\tau_{\perp}$) and tangential to the surface ($\tau_{\parallel}$) makes the contributions to the widths of the peaks as follows:

$$\delta\omega_{\parallel} = \lambda/(\tau_{\perp}\cos\theta_B), \quad \delta\omega_{\perp} = \lambda/(2\tau_{\parallel}\sin\theta_B), \quad (1)$$

for the symmetric Bragg layout and

$$\delta\omega_{\parallel} = \lambda/(\tau_{\perp}\cos\theta_B), \quad \delta\omega_{\perp} = \lambda/(2\tau_{\perp}\sin\theta_B). \quad (2)$$

for the symmetric Laue layout.

The asymmetric layout of the experiment allows the combination of the properties of the symmetric Bragg diffraction and Laue diffraction. Although the Laue diffraction provides a means of determining the distortion tensor component ε_{xx} just as it is, the X-ray diffraction experiment in the transmission mode of measurements can be carried out only for a limited group of slightly absorbing materials. It is known that the two-crystal reflectance curves obtained for two opposite-in-azimuth positions of the sample provide a possibility of determining ε_{zz} and ε_{xx}. In this case, the angle between the diffraction peaks of the film and substrate consists of two components, $\Delta\theta$ and $\delta\varphi$, of which the former characterizes the change in the interplanar spacing and the latter, the rotation of the atomic planes. Since the three-crystal diffractometry allows the separation of these effects, the analysis of the distribution of the diffraction signal in the ($q_{\parallel}$, $q_{\perp}$) coordinate system makes

it possible to determine each of the above two components separately [9].

Construction of the two-dimensional distribution of the signal intensity in the form of contours of equal intensities around the asymmetric Bragg peak makes it possible to establish directly the position of the reflectance centers of the layers in the scattering plane and to determine the coordinates $(q_\parallel, q_\perp)$ of each of them. In the case of a coherent interface between the film and wafer, the corresponding reciprocal lattice sites fall on the $q_\perp$ axis that passes through the site H_0. In the case of complete compensation of the stresses ($\varepsilon_{zz} = \varepsilon_{xx}$), we have $q_\perp = 0$, and the points H_1 and H_0 fall on the $q_\parallel$ axis. In the general case of partial relaxation, the site should be located in the acute sector formed by the diffraction vector and the normal to the surface that passes through the site H_0. However, in some circumstances, the point H_1 can be beyond this sector. First, this can occur if there are shear strains and rotations. Second, this can occur due to the effect of thermoelastic stresses, specifically, if the difference between the film and wafer in the thermal expansion coefficients $\Delta\alpha = \alpha_1 - \alpha_0$ is of the same sign as the mismatch between the lattice parameters $\Delta a = a_1 - a_0$. Third, unusual shifts of the center of reflection can be due to defects of packing. When we consider multilayered epitaxial structures, the above considerations should be related to the difference in the coordinates of the sites of the upper and lower adjacent layers, $\Delta q = q(j + 1) - q(j)$. In most actual cases, however, there is no need to obtain the complete pattern of the signal-intensity distribution. Instead, it is sufficient to construct two coordinate dependences along the diffraction vector (or the angular position of the analyzer), namely, the dependence of the integrated intensity of the ω peaks, $J(q_\parallel)$, and the dependence of the tetragonal distortion, $\delta\varphi$. The function $J(q_\parallel)$ does not account for the effect of rotations and bending and, as in the symmetric layout of the experiment, accounts only for the change in the interplanar spacing. This makes it possible to improve the resolution of the diffraction peaks produced by individual layers and to reliably record the angular position of the peaks [3].

The properties of the optical spectra of the samples were studied by means of laser-induced PL spectroscopy in a similar manner as was done previously [10]. Essentially, the diagnostis is that, on photoexcitation of interband transitions, the PL characteristics are controlled by the concentration of radiative and nonradiative states and by the transport of charge carriers towards these states. Therefore, the layers with different total concentrations of structural defects are inherently different in PL intensity, bandwidth, and energy positions of the peaks of emission.

The PL was excited by the monochromatic He–Cd laser radiation at the wavelength $\lambda = 325.0$ nm (corresponding to the photon energy $h\nu = 3.815$ eV) in the continuous-wave mode of operation (with the emission power 7 mW), which made it possible to maintain the excitation intensity constant. The PL spectra were recorded by a computer-controlled optical system that involved a scanning diffraction monochromator and a photomultiplier. The spectral resolution of the system was 0.02 meV. The PL signal was excited and detected on the opposite sides of the heteroepitaxial layers, both on the front side of the films and on the rear side of the wafer. The laser radiation was focused and directed at an angle of 45° to the sample surface and the PL radiation was collected in the orthogonal direction by lenses. In the experiments, the temperature of the samples was varied from 300 to 4.2 K; for this purpose, the samples were placed in an optical cryostat. In all optical measurements, we met the conditions of repetition and reproducibility of experiment to provide the correct relationships between the PL intensities and the correlation of the PL spectra.

3. RESULTS AND DISCUSSION

The X-ray diffraction studies of the GaN and AlGaN layers in different layouts of scanning show that the structural properties of the layers are different by virtue of various kinds of inhomogeneities, and confirm the stressed state of the HS under consideration. Figure 1 shows the X-ray diffraction spectra of samples S_1 (AlGaN/GaN) and S_2 (GaN), as obtained for the symmetric Bragg reflection when rocking around the 0002 reciprocal lattice site. As evident from Fig. 1, the intensity contours are extended along the direction orthogonal to the diffraction vector and have a shape typical of relaxed structures. The extension of the distribution of the intensity in the direction parallel to the surface is related to the anisotropy of the fields of elastic stresses in the heterolayers. The broadening of the reflection bands along the normal to the surface is much less pronounced.

The tangential dependence of the three-crystal curves of θ–2θ scanning for higher-order reflection bands suggests that the major contribution to the broadening of the reflection bands is made by strains [8]. The specific feature of the heterolayers under study is that, in the asymmetric $11\bar{2}4$ layout, the reflectance curves on grazing incidence are much narrower than those on grazing reflectance. Such a situation is characteristic of an extension of the reciprocal lattice site in the direction parallel to the surface. Since the diffraction vector components in the parallel and orthogonal directions are nearly equal for these reflections, the experimentally observed feature can be interpreted as a consequence of either the anisotropy of the components of microdistortion or the anisotropy of the CS regions (grains). The above-mentioned extension for sample S_1 is much more pronounced than that for sample S_2; the ratios of the half-widths of the curves are 0.45 and 0.71, respectively.

The microdistortion tensor components $\delta\varepsilon_{ij}$ that characterize different types of distortions of the crystal

lattice are listed in the table. The components were determined from the half-widths of the reflection bands for different layouts of the experiment. From these data, it follows that the dilatation component $\delta\varepsilon_{xx}$ is much larger than $\delta\varepsilon_{zz}$ and the orientation component $\delta\varepsilon_{zx}$ is larger than $\delta\varepsilon_{xz}$. The inequality $\delta\varepsilon_{xx} > \delta\varepsilon_{zz}$ suggests that local variations in the interplanar spacing between atomic planes orthogonal to the surface are substantially larger than those between atomic planes parallel to the interface. The relation $\delta\varepsilon_{zx} > \delta\varepsilon_{xz}$ (more pronounced for sample S_1 than for sample S_2) suggests that the planes parallel to the surface are characterized by larger angles of disorientation than the orthogonal planes. This allows us to relate the component $\delta\varepsilon_{zx}$ to threading screw dislocations that produce shearing strains and the component $\delta\varepsilon_{xx}$, to edge dislocations orthogonal to the heterointerface. As for the density of dislocations, it is approximately the same for edge dislocations and screw dislocations. The dimensions of grains, i.e., CS regions along the normal to the surface, are noticeably larger than those in the transverse dimensions: $\tau_z > \tau_z$. The parameters of the AlGaAs structure are much worse than those of GaN. However, it should be noted that the extensions of the distribution of the signal intensity around the 0002 reciprocal lattice site in the directions parallel to the surface and normal to the surface are virtually the same, which is caused by the uniformity of strains in all directions.

If we assume that $\tau_\perp$ is equal to the spacing between the levels of the dislocation network and $\tau_\parallel$ to the spacing between the dislocation lines in these networks, the resulting broadenings calculated by formulas (1) and (2) are found to be noticeably smaller than the experimental half-widths of the diffraction peaks. This circumstance suggests that, for the layers with dislocation networks, the major contributor to the peak broadening is the disorientation of CS regions; at the same time, with the linear density of the networks below 10^5 cm^{-1}, the contribution made by smaller-sized CS regions is much smaller. In addition, the planar configuration of the nets should not produce noticeable changes in the dimensions of the CS regions in the direction normal to the heterointerface. All these considerations lead us to the general conclusion that the prevalent effect of the dislocation networks is the broadening of the diffraction pattern in the direction orthogonal to the reciprocal lattice vector, irrespective of the layout of the experiment. This is consistent with the X-ray structural data for the epitaxial $Al_xGa_{1-x}N$ layers [8]. As to the effect
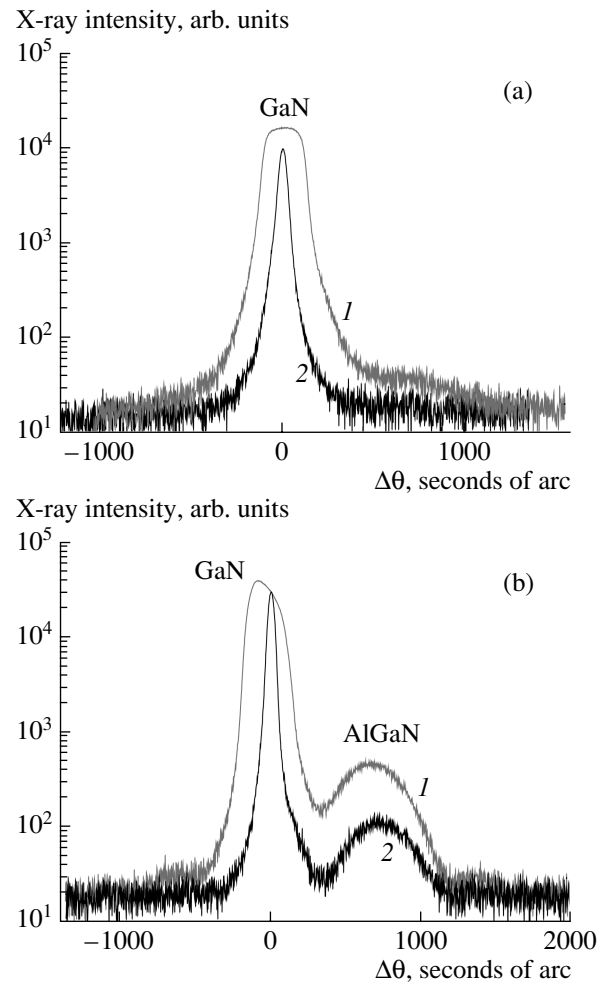

Fig. 1. X-ray diffraction rocking curves for the directions (*1*) orthogonal and (*2*) parallel to the diffraction vector of the symmetric 0002 reflection band for the (a) GaN/Al$_2$O$_3$(0001) and (b) AlGaN/GaN/Al$_2$O$_3$(0001) structures.

of the wafer structure, its manifestation in the spectra of X-ray diffraction scanning is only slightly pronounced. This effect can hardly be resolved, since the penetration depth of X-ray photons into the matrix is large and the formation of the X-ray diffraction pattern is of a three-dimensional character.

The PL studies of the GaN and AlGaN heterolayers at different temperatures in different experimental layouts of laser excitation supplement the X-ray diffrac-

Characteristics of the crystalline structure: the distortion tensor components $\delta\varepsilon_{ij}$, the dimensions of the regions of coherent scattering τ_z and τ_x, and the density of dislocation ρ in the epitaxial GaN and $Al_xGa_{1-x}N$ ($x = 0.25$) layers on the Al_2O_3 (0001) substrate

Sample, layer	$10^4\delta\varepsilon_{zz}$	$10^4\delta\varepsilon_{zx}$	$10^4\delta\varepsilon_{xz}$	$10^4\delta\varepsilon_{xx}$	τ_z, nm	τ_x, nm	ρ, 10^8 cm^{-2}
S_1, GaN	2.57	9.3	6.1	3.92	480	80	1.38
S_1, AlGaN	5.7	65	23	25	30	15	6.31
S_2, GaN	2.76	12.1	7.3	5.19	325	67	3.08

PL intensity, arb. units
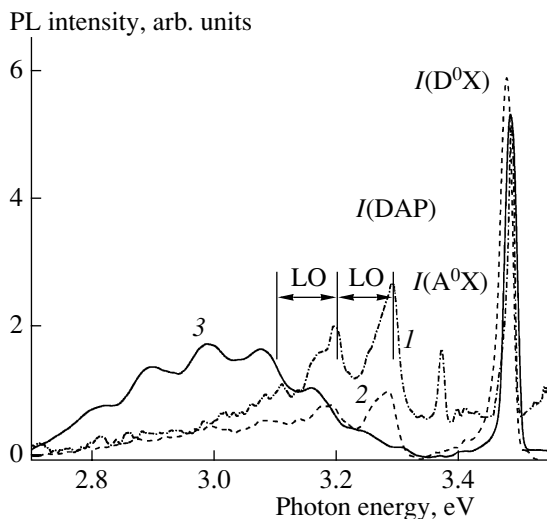
Fig. 2. PL spectra of the AlGaN/GaN/Al$_2$O$_3$ (S$_1$) and GaN/Al$_2$O$_3$ (S$_2$) samples at the temperature of 4.2 K. Curves *1–3* refer to the spectra for (*1*) sample S$_2$ with the front side photoexcited and (*2, 3*) sample S$_1$ with (*2*) the rear side and (*3*) front side photoexcited.

tion analysis and confirm the spatially nonuniform distribution of charge carriers over the energy bands and the nonuniform distribution of the impurity centers and defects inside the heterolayers.

Figure 2 shows the low-temperature (4.2 K) PL spectra of samples S$_1$ (the AlGaAs/GaN HS) and S$_2$ (the GaN film); the photon energies range from 2.7 to 3.5 eV. Common to all of the PL spectra are the high-energy portion formed by emission from the basic GaN layer and the low-energy portion formed by emission from the AlGaN–GaN heterointerface. The origin of the basic PL bands in GaN is well-known: these are due to radiative recombination of electron–hole pairs in the exciton complexes [11–14].

In Fig. 2, curve *1* represents the PL spectrum of sample S$_2$ (GaN) when the front side of the film is excited. The basic features of this spectrum are as follows: (i) the narrow $I(D^0X)$ emission line attributed to excitons bound to neutral donor centers, with a peak at $h\nu = 3.487$ eV (the full width at half-maximum is FWHM ≈ 10 meV); (ii) the $I(D^0X)$ line corresponding to emission of excitons bound to acceptor centers, with the peak at $h\nu = 3.375$ eV (FWHM ≈ 10 meV); and (iii) the asymmetric $I(DAP)$ band that is peaked at $h\nu = 3.29$ eV (FWHM ≈ 40 meV) and corresponds to the donor–acceptor recombination of shallow donor–acceptor pairs (DAPs), with a minor component of electron–acceptor recombination (e, A). The spectral curves exhibit peaks at $h\nu = 3.20$ and 3.11 eV corresponding to the LO and 2LO optical phonon replicas due to electronic transitions in the DAPs (the LO phonon energy is $h\nu_{LO} \approx 90$ meV). In addition, there are some low-intensity lines of excitonic emission around $h\nu = 3.42$ eV, related to impurity complexes and struc-

tural defects at the misfit dislocations in the epitaxial films [8].

In Fig. 2, curve *2* represents the PL spectrum of sample S$_1$ (AlGaN/GaN) in the case where the rear side of the wafer (i.e., the side of the GaN layer) is excited. It can be seen that this spectrum replicates the basic features of the PL spectrum of sample S$_2$ (GaN), with the exception of the $I(A^0X)$ exciton–acceptor line that is lacking in the case of sample S$_1$. Here, the prevailing line is the $I(D^0X)$ exciton–donor peak at the energy $h\nu = 3.49$ eV (FWHM ≈ 17 meV) corresponding to the band gap of GaN.

In Fig. 2, curve *3* represents the PL spectrum of sample S$_1$ (AlGaN/GaN) in the case where the front side (i.e., the side of the AlGaN layer) is excited. It is evident that, in this layout of photoexcitation, the PL spectrum is modified. In this case, a broad intense PL band appears in the low-energy spectral range from 2.7 to 3.3 eV (FWHM ≈ 0.35 eV). This band exhibits an internal structure (peaks at $h\nu = 2.90$, 3.00, 3.08, and 3.17 eV) whose origin can be attributed to recombination of donor–acceptor pairs produced by structural defects at the AlGaN–GaN heterointerface and by impurity centers in the GaN heterolayer. At the same time, the $I(D^0X)$ PL band, with a peak at $h\nu = 3.49$ eV in the edge region of the spectrum, remains in the same position, and the $I(A^0X)$ band is lacking.

Thus, on photoexcitation of the AlGaN/GaN/Al$_2$O$_3$ HS on the rear side of the HS, we observe the PL spectrum typical of the GaN films. Since the laser excitation is completely absorbed within the thickness of the GaN layer, the PL spectra of different samples differ little in shape. The effect of structural defects in the GaN layer and at the Al$_2$O$_3$–GaN interface is nearly the same; therefore, the intensity and peak position of the $I(D^0X)$ PL band ($h\nu = 3.49$ eV) remain virtually unchanged. The slightly larger FWHM of the edge band suggests a smaller degree of structural quality of the layer in the HS compared to the individual epitaxial film. The PL via localized states at the AlGaN–GaN heterointerface is not observed here.

On photoexcitation of the AlGaN/GaN/Al$_2$O$_3$ HS at the front side, the shape of the PL spectrum is substantially changed, representing the kinetics of charge carriers in the doped AlGaN barrier layer and the formation of quasi-two-dimensional electron gas in the AlGaN–GaN heterointerface region at high concentration of dopant centers and high density of dislocations in the GaN heterolayer. The absolute value of the PL intensity becomes larger by an order of magnitude. This is consistent with the well-known fact that, for doped GaN, the intensity of the edge $I(D^0X)$ PL band in the spectrum is typically higher than that for undoped GaN and the peak is shifted to shorter wavelengths compared to that for undoped GaN. As a result, new deep levels that trap photoexcited carriers are produced in the band gap. The trapping brings about a substantial decrease in the lifetime of free holes, and therefore, the features

corresponding to recombination of quasi-two-dimensional electrons with free holes at the heterointerface are not observed in the PL spectrum. However, the concentration of photoexcited holes bound to the extra acceptor centers becomes much higher, and this tends to enhance the radiative recombination of DAPs in the low-energy part of the spectrum.

As temperature is increased, the intensity of the high-energy portion of the PL spectrum decreases, suggesting higher rates of nonradiative recombination processes, and the PL band as such becomes broader because of termalization of the energy distribution of electrons. The low-energy part of the PL spectrum shifts further to lower energies. This shift is attributed to the higher mobility of charge carriers in doped AlGaN/GaN structure compared to the mobility in the undoped GaN layer.

4. CONCLUSIONS

Summarizing, in this study, we apply X-ray diffractometry and PL optical spectroscopy to the comprehensive experimental analysis of the properties of epitaxial layers in the HEMT $Al_xGa_{1-x}N$ ($x = 0.25$) HS grown by the MOCVD process on (0001)-oriented single crystal sapphire. The X-ray structural data (the characteristics of diffraction reflections) show that, in the GaN and ALGaN layers, there exist internal microstresses and structural inhomogeneities. These are produced due to some features of the technological procedure and composition of the structure, including features related to the heavily doped sublayer for the barrier AlGaN layer. The highest density of dislocations (from 1×10^8 to 7×10^8 cm^{-2}), as well as the largest stresses, are detected at the AlGaN–GaN heterointerface. The nonuniform distribution of stresses and dislocations may be responsible for the difference between the PL spectra of GaN and AlGaN/GaN (in energy position, width, and intensity of the emission lines). In both cases, photoexcitation of GaN is of interband character; however, the dopant centers draining towards dislocations at the AlGaN–GaN hetrointerface produce new deep levels in the band gap, which trap photoexcited charge carriers. As a result, along with the excitonic PL peak in the edge spectral region ($h\nu = 3.49$ eV), a broad intense PL band appears in the low-energy region of the spectrum (from 2.7 to 3.3 eV). This low-energy band is attributed to the recombination of DAPs involving extra acceptor centers. We assume that the experimentally observed effects are also due to some specific features of the formation of quasi-two-dimensional electron gas in the heterointerface region.

The results obtained here may prove useful for developing semiconductor devices that involve epitaxial HSs based on the AlGaN/GaN-type materials.

REFERENCES

1. Zh. I. Alferov, Fiz. Tekh. Poluprovodn. (St. Petersburg) **32**, 3 (1998) [Semiconductors **32**, 1 (1998)].

2. V. A. Kochelap, V. V. Mitin, and M. A. Stroscio, *Quantum Heterostructures: Microelectronics and Optoelectronics* (Cambridge Univ. Press, Cambridge, 1999).

3. L. A. Datsenko, V. F. Machulin, V. P. Klad'ko, and V. B. Molodkin, *X-ray Dynamic Scattering by Real Crystals in the Region of Anomalous Dispersion* (Akademperiodika, Kiev, 2002) [in Russian].

4. H. [!]Morkoc, *Nitride Semiconductors and Devices* (Springer, Berlin, 1999).

5. B. A. Danilchenko, S. E. Zelensky, E. Drok, et al., in *Proceedings of 6th International Conference on Nitride Semiconductors* (Bremen, Germany, 2005); Appl. Phys. Lett. **85**, 5421 (2004).

6. V. V. Lundin, E. E. Zavarin, A. I. Besyul'kin, et al., Fiz. Tekh. Poluprovodn. (St. Petersburg) **38**, 1364 (2004) [Semiconductors **38**, 1323 (2004)].

7. V. P. Klad'ko, L. I. Datsenko, P. M. Litvin, et al., Semicond. Phys. Quantum Electron. Optoelectron. **4**, 146 (2001).

8. V. V. Ratnikov, R. N. Kyutt, T. V. Shubina, et al., J. Phys. D: Appl. Phys. **34** (10A), A30 (2001).

9. A. S. Usikov, V. V. Tret'yakov, A. V. Bobyl', et al., Fiz. Tekh. Poluprovodn. (St. Petersburg) **34**, 1300 (2000) [Semiconductors **34**, 1248 (2000)].

10. A. V. Naumov, A. E. Belyaev, and A. V. Komarov, in *Proceedings of 5th International Conference on Problems of Optics and High Technology Material Science, SPO 2004* (Kiev, Ukraine, 2004), p. 182.

11. B. Monemar, Mater. Sci. Eng. B **59**, 122 (1999).

12. S. Y. Fang, C. F. Lin, E. Y. Chang, and M. S. Feng, Appl. Phys. Lett. **80**, 742 (2002).

13. V. V. Ursaki, I. M. Tiginyanu, V. V. Zalamai, et al., J. Appl. Phys. **94**, 4813 (2003).

14. P. P. Paskov, R. Schifano, B. Monemar, et al., J. Appl. Phys. **98**, 093 519 (2005).

Translated by É. Smorgonskaya

SPELL: 1. diffractometry, 2. photoexcited, 3. heterointerface, 4. broadenings, 5. diagnostis, 6. interband, 7. microdistortion, 8. termalization, 9. microstresses, 10. hetrointerface